Int. J. Electrochem. Sci., 16 **(2021)** Article ID: 210320, doi: 10.20964/2021.03.12

International Journal of
ELECTROCHEMICAL
SCIENCE
www.electrochemsci.org

Short Communication

Nitrogen-doped NiO prepared by magnetron sputtering and its electrochemical performance as an electrode material for supercapacitors

Guihua Wang[#,1], *Rusheng Wei*[#,2], *Lianguo Gong*[1], *Yuan Tian*[1,3,*], *Hongming Fei*[3], *Yibiao Yang*[1,*], *Xiaodan Zhao*[3]

[1] Key Lab of Advanced Transducers and Intelligent Control System, Ministry of Education, Taiyuan University of Technology, Taiyuan 030024, PR China
[2] Shanxi Semicore Crystal Co., Ltd., Taiyuan, 030024, PR China
[3] College of Physics and Optoelectronics, Taiyuan University of Technology, Taiyuan, 030024, PR China
[*]E-mail: tiantianquan0901@126.com, yangyibiao_tyut@sohu.com
[#] Guihua Wang and Rusheng Wei are co-first authors of the article.

Received: 27 October 2020 / *Accepted:* 16 December 2020 / *Published:* 31 January 2021

NiO is a very promising electrode material for supercapacitors. However, its poor cycle stability and low conductivity hinder its application. Here, we report the fabrication of nitrogen-doped NiO thin films prepared by reactive radiofrequency magnetron sputtering in a N_2 and Ar gas mixture and further their applications for supercapacitors for the first time. SEM was used to analyze the morphology changes of the NiO films. XRD and XPS were performed to characterize the structure and elemental composition, respectively. The variation in supercapacitor performance with N_2 content was evaluated. With increasing N_2 percentage, the NiO conductivity was found to be improved, while the specific capacitance was increased. A NiO thin film prepared at 80% N_2 was analyzed; compared with the pure NiO film, the specific capacitance was increased by approximately 5 times (13.4 to 61.6 mF/cm^2) at 1.0 mA cm^{-2}; after 10000 cycles, the capacitance retention was higher than 100% (104%). As a consequence, nitrogen-doped NiO prepared by magnetron sputtering demonstrates great potential as a promising supercapacitor electrode material.

Keywords: NiO; Nitrogen doping; Magnetron sputtering; Supercapacitors

1. INTRODUCTION

Transition metal oxides have been intensively studied as promising electrochemical materials for supercapacitors with the advantages of an environmentally friendly nature, multiple oxidation and high theoretical specific capacitance. [1-3] Among such materials, nickel oxide (NiO) has attracted

considerable attention as a p-type electrode. [4] Various strategies have been employed to synthesize NiO, such as sol-gel [5, 6], electron beam evaporation [7, 8], pulsed laser deposition [9], magnetron sputtering [10] and hydrothermal synthesis [11]. Magnetron sputtering is a widely used method for surface coating [12] and functional materials [13-15]. During the past few years, magnetron sputtering has been extended to electrode preparation with the facility of forming large-scale thin films on complex and flexible surfaces with better adhesion. [16-17] Binbin Wei et al fabricated a CrN film electrode using reactive DC magnetron sputtering, which shows a specific capacitance of 12.8 mF cm^{-2} at 1.0 mA cm^{-2} and high cycling stability with 92.1% capacitance retention after 20 000 cycles in a 0.5 M H_2SO_4 electrolyte [18]. B Wei et al. studied the electrochemical properties of TiN thin films. These films showed a capacitance of 27.3 mF cm^{-2} at a current density of 1.0 mA cm^{-2}, and a capacitance retention of 98.2% after 20,000 cycles at 2.0 mA cm^{-2}. [19]

Many reports have clarified the effect of doping on capacitance and stability. [20, 21] This effect enhances the competitive advantage of magnetron sputtering, with which continuous regulation of the doping concentration can be achieved by cosputtering and reactive sputtering. [22] In this paper, we significantly improve the electrochemical performance of NiO by nitrogen doping with magnetron sputtering. The specific capacitance reaches 61.6 mF/cm^2, which is prominent for a film electrode.

2. EXPERIMENTAL PART

2.1. Materials and sample preparation

NiO thin films were deposited onto transparent ITO glass substrates (sheet resistance value: 12 Ω·cm, size: 2 cm×2 cm) by reactive radiofrequency magnetron sputtering. The substrates were successively cleaned with soapy water, alcohol and deionized water. A NiO ceramic target (99.99% purity) of 6 cm was adopted. The distance between the target and substrate remained at 5 cm during the sputtering process. The initial chamber pressure was 2×10^{-5} Pa, and the working pressure was 1 Pa. The sputter power was maintained at 140 W. The substrates were heated and maintained at 400°C during sputtering. Five NiO thin films were deposited in different gases: Ar, 80% Ar / 20% N_2, 60% Ar / 40% N_2, 40% Ar / 60% N_2 and 20% Ar / 80% N_2. The thickness of the NiO films was 200 nm, as determined by an INFICON STM-2XM thickness monitor.

2.2. Characterization

Hitachi S4800 field emission scanning electron microscopy (FE-SEM) was used to characterize the surface morphology of the resulting films. A Philips X'pert PRO X-ray diffractometer (XRD) equipped with Cu Kα radiation was adopted to analyze the structure. X-ray photoelectron spectroscopy (XPS) measurements were performed using a Thermo ESCALAB 250XI with Al Kα radiation.

2.3. Electrochemical measurements

The electrochemical performance of NiO thin films was evaluated using a traditional three-electrode glass cell connected to an electrochemical workstation. A platinum electrode (1 cm^2) and a saturated calomel electrode (SCE) were selected as the counter electrode and reference electrode, respectively. Cyclic voltammetry (CV) measurements at a series of scan rates ranging from 2 mV/s to 100 mV/s in a potential window of 0 V to 0.4 V were performed in a 6.0 M KOH aqueous solution. Galvanostatic charge-discharge tests (GCDs) were performed at different current densities. The areal capacitance (C_a) was calculated using the following equation:

$$C_a = I \times t / (\Delta V \times S)$$

where I is the constant discharge current, t is the discharge time, ΔV is the voltage drop during discharging (excluding the IR drop) and S is the area of the NiO thin films. Electrochemical impedance spectroscopy (EIS) tests were carried out with an AC potential amplitude of 5 mV over the frequency range of 100 kHz - 0.1 Hz.

3. RESULTS AND DISCUSSION

Figure 1 shows plan-view SEM images of NiO films at different gases. The surfaces consist of many inhomogeneous small grains and are relatively compact. The evolution of the morphologies is evident. With increasing N_2 content, the grain size gradually decreases. When the N_2 percentage is 80%, some of the grains are too small to distinguish. Meanwhile, the flatness of the films improves as N_2 increases.

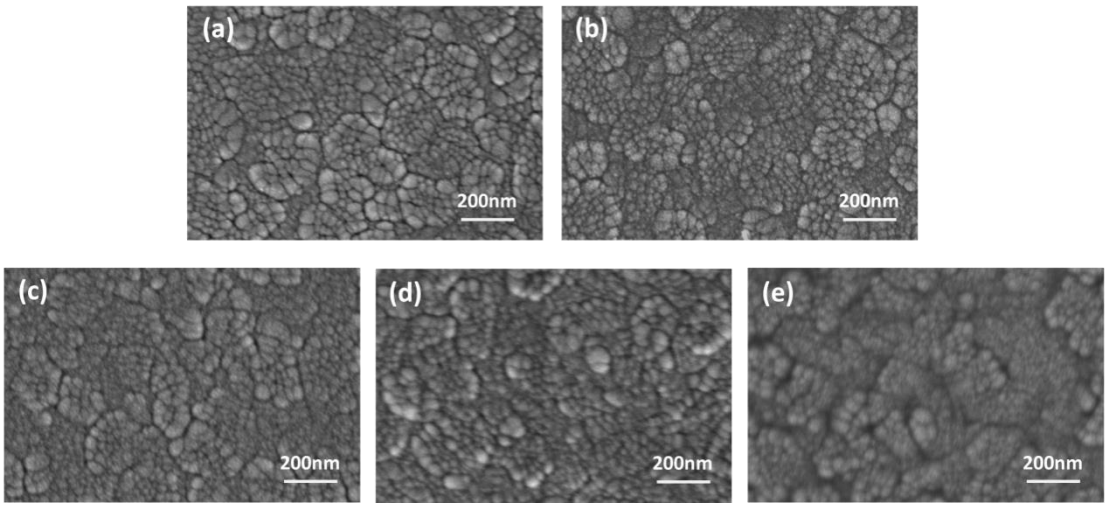

Figure 1. Plan view SEM images of NiO films at different gases: 100% Ar (a), 80% Ar / 20% N_2 (b), 60% Ar / 40% N_2 (c), 40% Ar / 60% N_2 (d) and 20% Ar / 80% N_2 (e).

XRD characterization was adopted to analyze the crystal structure of the NiO films. The XRD measurement demonstrated that the NiO films had a cubic fcc structure (JCDPS No. 47-1049). The

main diffraction peaks observed near 37.36° and 61.7° are assigned to NiO (111) and NiO (220), respectively. The other peaks are corresponding to the ITO layers [23]. The height ratio between NiO (111) and NiO (220) indicates the preference of the NiO <111> orientation. The NiO (111) peak shifts towards a higher angle as the N_2 percentage increases from 0% to 60%, corresponding to smaller lattice parameters. When the N_2 percentage is 80%, the (111) peak shifts to a lower angle, indicating an expansion of the framework. As the Ni-N bond distances (2.26 Å) are longer than Ni-O (2.11 Å) [24], the increase in nitrogen incorporation is expected to result in larger lattice parameters. The abnormality of NiO at 0% to 60% N_2 may be due to the residual stress present in the films.

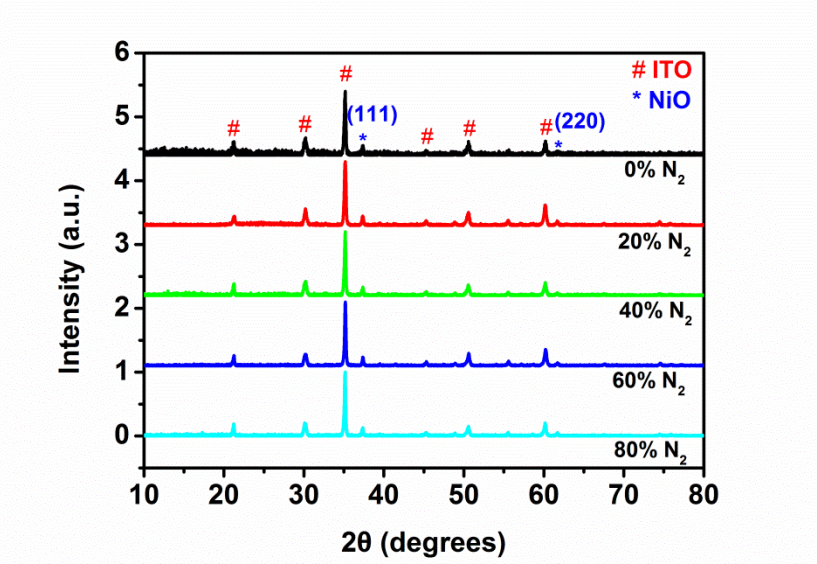

Figure 2. XRD diffraction patterns for NiO with varying N_2 percentage.

The CV curves acquired from different NiO thin films at a scan rate of 50 mV/s are shown in Fig. 3a. Notably, the integral area of the CV file increases with N_2 percentage, thus indicating that nitrogen doping improves electrochemical reaction activity. Sample T1 is close to rectangular curves, and the redox peaks are very weak, corresponding to the main effects of electric double-layer capacitance (EDLC). As the N_2 percentage increases, redox peaks become increasingly obvious, indicating reversion of the storage mechanism from electric double-layer capacitance to faradaic pseudocapacitance. The formation of redox peaks is attributed to the reactions between the electrode material and alkaline electrolyte. The reaction equation is as follows: [25]

$$Ni^{II} + OH^- \leftrightarrow Ni^{III} + e^- \quad (1)$$

GCD curves of NiO films prepared at a series of N_2 percentages were obtained at a current density of 1.0 mA/cm^2 within the potential window of 0 V to 0.38 V. For the pure NiO film, the GCD curves approach symmetry, indicating that the predominance of electric double-layer physisorption contributes. With increasing nitrogen doping, the shoulders of the GCD curves become obvious, which is attributed to an enhanced pseudocapacitance contribution. The areal capacitances of the NiO samples calculated from the GCD curves are shown in Fig. 3c. The areal capacitance increases from 13.4 mF/cm^2 to 17.5 mF/cm^2 to 22.2 mF/cm^2 to 34.2 mF/cm^2 to 61.6 mF/cm^2 as the N_2 percentage changes from 0% to 20% to 40% to 60% to 80%, respectively. The values of areal capacitance for different films reported in literature are demonstrated in Table 1.

Table 1. Areal capacitance of different films from literature.

Film	Method	Substrate	Electrolyte	Current Density (mA cm^{-2})	Scan Rate (mV s^{-1})	Areal Capacitance (mF cm^{-2})	Reference
RuO_2	Electro-deposition	Ti	0.5 M H_2SO_4	5	-	1.92	[26]
V_2O_5	Physical Vapor Deposition	FTO	2 M KOH	-	10	9.7	[27]
CrN	Magnetron sputtering	Si (100) wafers	0.5 M H_2SO_4	1.0	-	12.8	[18]
$MnO_{1.9}$	Magnetron sputtering	Copper	0.5 M Na_2SO_4	1.0	-	23.3	[28]
TiN	Magnetron sputtering	Si (100) wafers	0.5 M H_2SO_4	1.0	-	27.3	[19]
MoO_x ($2.3 < x < 3$)	Magnetron sputtering	FTO	-	-	5	31	[29]
4% Mo-doped V_2O_5	Thermal evaporation	Nickel	1 M KCl	-	10	83	[30]
2%Mo-doped WO_3	Electro-deposition	FTO	1 M $LiClO_4$/PC	-	10	117	[31]

Nitrogen doping of the NiO film also helps to improve the conductivity, as supported by electrochemical impedance spectroscopy (EIS). The Nyquist plots for NiO films in the frequency range from 100 kHz to 0.1 Hz are shown in Fig. 3d. The semicircular shape of the EIS spectra in the low-frequency region is demonstrated as an inset picture. The diameter of the semicircle decreases with N_2 percentage, which means increasing charge transfer resistance.

Considering its excellent electrochemical performance, a NiO thin film at 80% N_2 was chosen for further study. The elemental composition and states were characterized by XPS. XPS survey spectra, demonstrated in Fig. 4a, reveal the peak characteristics of nickel, oxygen, nitrogen and carbon. The Ni 2p spectra, shown in Fig. 4b consist of six components. The fitting peaks at 855.2 eV and 873.1 eV are assigned to Ni^{2+}. In addition, the peak at approximately 861.1 eV is its satellite (sat.) peak. The fitting peak at 856.8 eV is assigned to Ni^{3+}, which conventionally appears at the NiO surface. [32] A shakeup-type satellite peak for $Ni2p_{1/2}$ is detected at 879.3 eV. The peak at 866.3 eV is assigned to the $c3d^{10}L^2$ final state configuration. [33] The O 1 s spectra (Fig. 4c) show two peaks at 528.9 eV and 531 eV, confirming the formation of Ni-O and Ni_2O_3. [34] Figure 4d depicts N 1 s spectra. The peaks located at 396 eV and 397.4 eV are attributed to atomic N in the Ni oxide lattice [35] and N atoms bonded to O [36], respectively. The other two peaks at 399.8 eV and 403 eV may be attributed to nitrogen atoms related to N-O bonds due to surface oxidation and ammonium-type bonds[37-39].

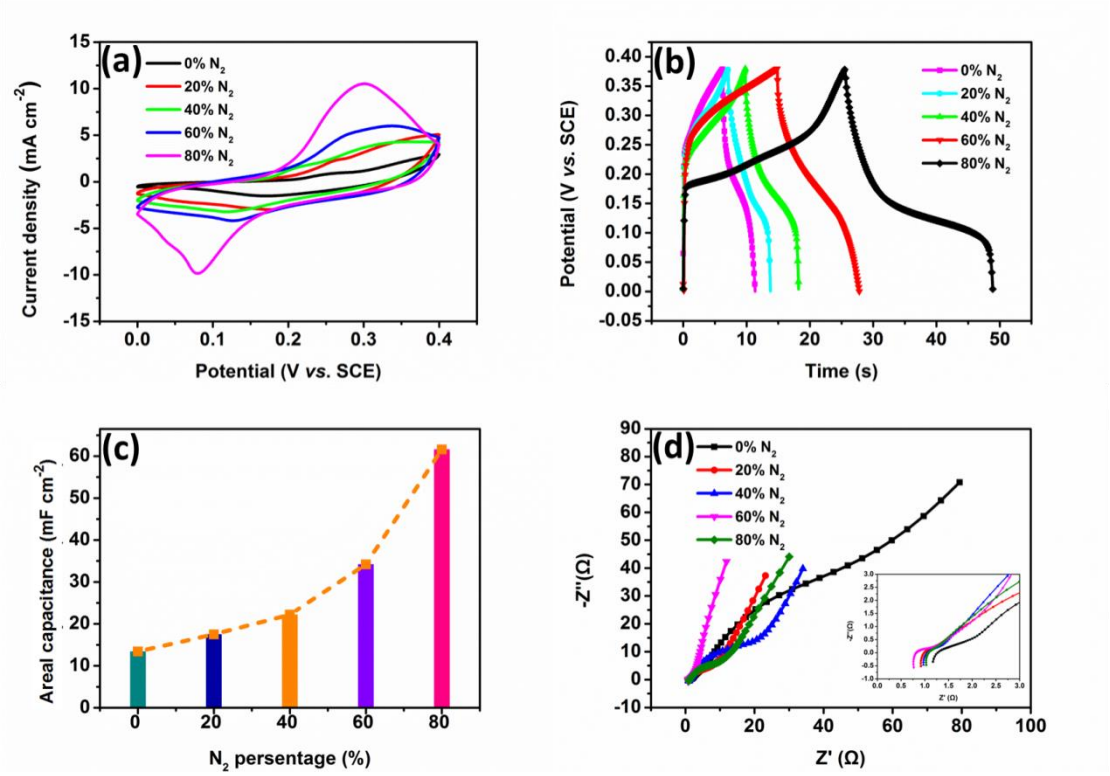

Figure 3. CV curves (a), GCD curves (b), areal capacitance (c) and Nyquist plot for NiO thin films as a function of N_2 percentage.

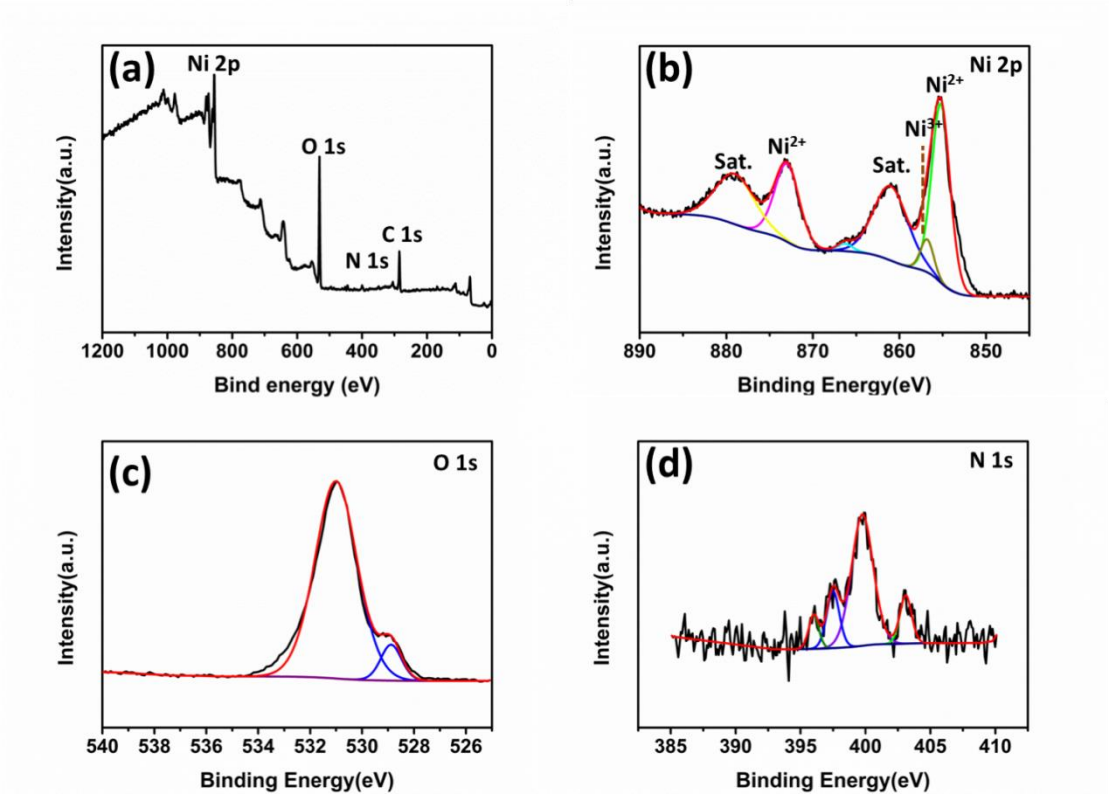

Figure 4. XPS survey spectra (a), Ni 2p spectra (b), O 1 s spectra (c) and N 1 s spectra (d) for NiO thin films at 80% N_2.

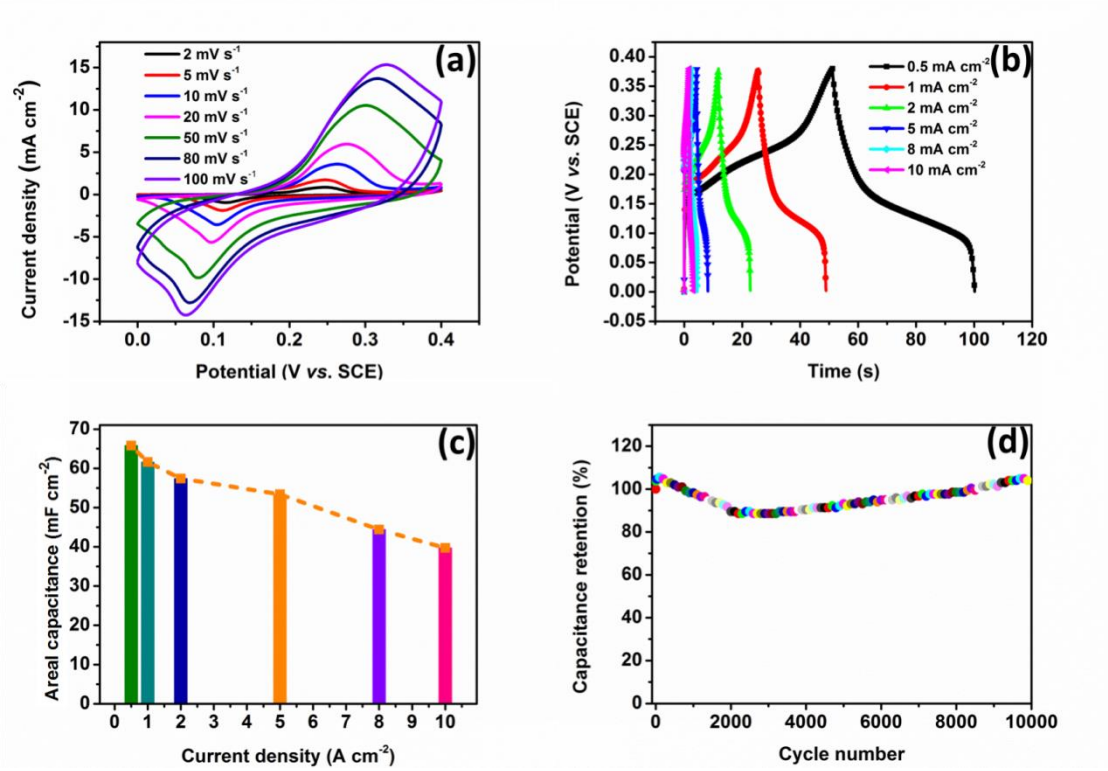

Figure 5. CV curves at different scan rates (a), GCD curves at different curve densities (b), areal capacitances at different curve densities (c) and cycle capabilities of the NiO film at 80% N_2.

Figure 5a shows the CV curves of the NiO film prepared at 80% N_2 measured at different scan rates. The symmetrical redox peaks reveal good reversibility and dominance of the pseudocapacitance contribution. The peaks reveal good kinetic reversibility at a large scan rate. With increasing scan rate, the cathodic peaks shift from 0.12 V to 0.07 V and the anodic peaks shifts from 0.24 V to 0.33 V. Electron hopping resistance to ion and electron transfer at higher scan rates is responsible for this shift. [1]

The shoulders of the GCD curves at 0.25 V during charging and 0.15 V during discharging indicate redox reactions, which is consistent with the CV analysis. The GCD curves are nearly symmetric, indicating excellent reversible redox reactions. The discharge capacitance is shown in Fig. 5c. The areal capacitance transforms from 65.8 mF cm^{-2} to 61.6 mF cm^{-2} to 57.4 mF cm^{-2} to 53.4 mF cm^{-2} to 44.4 mF cm^{-2} to 39.7 mF cm^{-2} at 0.5 mA cm^{-2}, 1 mA cm^{-2}, 2 mA cm^{-2}, 5 mA cm^{-2}, 8 mA cm^{-2}, and 10 mA cm^{-2}, respectively, revealing good rate capability with 60% capacitance retention when the current density increases by 20 times. The cycle capability was measured for 10000 cycles at a current density of 5 mA cm^{-2}. The areal capacitance of the NiO thin films increases by 5.5% after the first 100 cycles, which is attributed to the activation process of the NiO electrode. After the first 100 cycles, the specific capacitance begins to decline. When the cycle number is 2000, the capacitance retention reaches a minimum value. As the charge/discharge process continues, the specific capacitance increases and reaches 104% at 10000 cycles, revealing excellent cycling stability. This phenomenon can be explained by an increase in surface area due to surface corrosion during the redox reaction.

4. CONCLUSIONS

NiO thin films with varying N_2 contents were prepared by radio-frequency reactive magnetron sputtering at 400°C. The electrochemical performance was detected in a 6.0 M KOH aqueous solution. A NiO film prepared at 80% N_2 had the best electrochemical properties. With increasing N_2 percentage, the specific capacitance increased by approximately 5 times (from 13.4 mF/cm^2 to 61.6 mF/cm^2). The nitrogen doping of NiO at 80% N_2 was further studied. XPS measurements demonstrated the incorporation of N atoms into the NiO lattice. The film retains 60% capacitance when the current density increases by 20 times. Meanwhile, it possesses excellent cycle stability. After 10000 cycles, instead of decreasing, the capacitance retention increases to 104%. According to our research, Nitrogen doping by magnetron sputtering is an effective method to improve the electrochemical performance of NiO.

ACKNOWLEDGEMENTS
This work was supported by the National Natural Science Foundation of China (Contract No. 51702226, 11904255).

References

1. S. Wu, K.S. Hui, K.N. Hui and K.H. Kim, *J. Mater. Chem. A*, 4 (2016) 9113.
2. Q. Yang, Z. Lu, Z. Chang, W. Zhu and X. Duan, *RSC Adv.*, 2 (2012) 1663.
3. Q. Li, Z.L. Wang, G.R. Li, R. Guo, L.X. Ding and Y.X. Tong, *Nano Lett.*, 12 (2012) 3803.
4. W.L. Jang, Y.M. Lu, W.S. Hwang, T.L. Hsiung and H.P. Wang, *Appl. Phys. Lett.*, 94 (2009) 062103.
5. Z. Zhu, Y. Bai, T. Zhang, Z. Liu, X. Long, Z. Wei, Z. Wang, L. Zhang, J. Wang, F. Yan and S. Yang, *Angew. Chem. Int. Ed.*, 126 (2014) 12779.
6. T. Sreethawong, Y. Suzuki and S. Yoshikawa, *Int. J. Hydrogen Energy*, 30 (2005) 1053.
7. D.Y. Jiang, J.M. Qin, X. Wang, S. Gao, Q.C. Liang and J.X. Zhao, *Vacuum*, 86 (2012) 1083.
8. S. Pereira, A. Gonçalves, N. Correia, J. Pinto, L. Pereira, R. Martins and E. Fortunato, *Sol. Energy Mater. Sol. Cells*, 120 (2014) 109.
9. J.H. Park, J. Seo, S. Park, S.S. Shin, Y.C. Kim, N.J. Jeon, H.W. Shin, T.K. Ahn, J.H. Non, S.C. Yoon and C.S. Hwang, *Adv. Mater.*, 27 (2015) 4013.
10. M. Guziewicz, J. Grochowski, M. Borysiewicz, E. Kaminska, J.Z. Domagala, W. Rzodkiewicz, B.S. Witkowski, K. Golaszewska, R. Kruszka, M. Ekielski and A. Piotrowska, *Opt. Appl.*, 41 (2011) 431.
11. P. Justin, S.K. Meher and G.R. Rao, *J. Phys. Chem. C*, 114 (2010) 5203.
12. M. Neuhaeuser, H. Hilgers, P. Joeris, R. White and J. Windeln, *Diamond Relat. Mater.*, 9 (2000) 1500.
13. S. Mahadeva, J. Fan, A. Biswas, K. Sreelatha, L. Belova and K. Rao, *Nanomaterials*, 3 (2013) 486.
14. M. Desai, S. Prasad, N. Venkataramani, I. Samajdar, A.K. Nigam and R. Krishnan, *J. Magn. Magn. Mater.*, 246 (2002) 266.
15. K.S. Usha, R. Sivakumar, C. Sanjeeviraja, V. Sathe, V. Ganesan and T.Y. Wang, *RSC Adv.*, 6 (2016) 79668.
16. N. Choudhary, D.K. Kharat and D. Kaur, *Surf. Coat. Technol.*, 205 (2011) 3387.
17. N. Choudhary, J. Park, J.Y. Hwang and W. Choi, *ACS Appl. Mater. Interfaces*, 6 (2014) 21215.
18. B. Wei, H. Liang, D. Zhang, Z. Wu, Z. Qi and Z. Wang, *J. Mater. Chem.*, 5 (2017) 2844.
19. B. Wei, H. Liang, D. Zhang, Z. Qi, H. Shen and Z. Wang, *Mater. Renewable Sustainable Energy*, 7 (2018) 11.

20. L. Zhao, L.Z. Fan, M.Q. Zhou, H. Guan, S. Qiao, M. Antonietti and M.M. Titirici, *Adv. Mater.*, 22 (2010) 5202.
21. L.F. Chen, X.D. Zhang, H.W. Liang, M. Kong, Q.F. Guan, P. Chen, Z.Y. Wu and S.H. Yu, *ACS Nano*, 6 (2012) 7092.
22. C. Shi, H. Li, C. Li, M. Li, C. Qu and B. Yang, *Appl. Surf. Sci.*, 357 (2015) 1380.
23. J. Qiu, Z. Chen and T. Zhao, *J. Nanosci. Nanotechnol.*, 18 (2018) 4222.
24. M. Nolan, R. Long, N.J. English and D.A. Mooney, *J. Chem. Phys.*, 134 (2011) 224703.
25. Q. Lu, M.W. Lattanzi, Y. Chen, X. Kou, W. Li, X. Fan, K.M. Unruh, J.G. Chen and J.Q. Xiao, *Angew. Chem. Int. Ed.*, 50 (2011) 6847.
26. C. D. Lokhande, B. O. Park, H. S. Park , K. D. Jung and O. S. Joo, *Ultramicroscopy, 105* (2005) 267.
27. R. Velmurugan, J. Premkumar, R. Pitchai, M. Ulaganathan and B. Subramanian, *ACS Sustainable Chem. Eng., 7* (2019) 13115.
28. Li, Y. , Xie, H. , Li, J. , & Wang, J. *Mater. Lett.*, 102 (2013) 30.
29. C. Liu, Z. Li and Z. Zhang, *Sci. Technol. Adv. Mater., 14* (2013) 065005.
30. N. G. Prakash, M. Dhananjaya, B.P.Reddy, K.S. Ganesh, A.L.Narayana, O.M.Hussain, *Mater. Today*, 3 (2016) 4076.
31. S. Xie, Z. Bi, Y. Chen, X. He, X. Guo, X. Gao and X.Li, *Appl. Surf. Sci.*, 459 (2018) 774.
32. Y. Lei, J. Li, Y. Wang, L. Gu, Y. Chang, H. Yuan and D. Xiao, *ACS Appl. Mater. Interfaces*, 6 (2014) 1773.
33. S. Hüfner, F. Hulliger, J. Osterwalder and T. Riesterer, *Solid State Commun.*, 50 (1984) 83.
34. B. Sasi and K.G. Gopchandran, *Nanotechnology*, 18 (2007) 115613.
35. R. Asahi, T. Morikawa, T. Ohwaki, K. Aoki and Y. Taga, *science*, 293 (2001) 269.
36. K.R. Wu and C.H. Hung, *Appl. Surf. Sci.*, 256 (2009) 1595.
37. S. Aduru, S. Contarini and J.W. Rabalais, *J. Phys. Chem.*, 90 (1986) 1683.
38. P. Simon, B. Pignon, B. Miao, S. Coste-Leconte, Y. Leconte, S. Marguet, P. Jegou, B. Bouchet-Fabre, C. Reynaud and N. Herlin-Boime, *Chem. Mater.*, 22 (2010) 3704.
39. D.A. Duarte, J.C. Sagás, A.S. da Silva Sobrinho and M. Massi, *Appl. Surf. Sci.*, 269 (2013) 55.